Supporting Information

MXene-Integrated Ni–Co Telluride Composites as Restacking-Free Electrodes for Boosted Pseudocapacitive Performance

Vanjinayaki Paulraj, Sureka Kanthasamy Selvaraju Thangavelu*

Department of Chemistry, Bharathiar University, Coimbatore – 641 046, India.

* Email: veluselvaraju@gmail.com; selvaraju@buc.edu.in

Characterization techniques

X-ray diffraction (XRD) pattern analysis was performed for the prepared materials using Shimadzu XRD-6000, Japan with Cu Kα (λ =1.5416 Å) radiation at the scanning limit of 2θ = 10º to 90º and a scanning speed of 10º min^{-1}. The FT-IR spectrometer (FTIR, Bruker, TENSOR 27 spectrometer) was used to gather the vibrational frequencies of the prepared $NiCoTe_2$/MXene composite. The Brunauer-Emmett-Teller (BET) (Micro-Trac BELCORP, Japan) analyzer was used to evaluate the specific surface area and the Barrett-Joyner-Halenda (BJH) framework was used to investigate the pore volume distributions of the prepared materials. Field Emission Scanning Electron Microscopy (FESEM) (FEI quanta 250-FESEM, Bruker, Germany) with EDAX mapping analysis predicted the surface morphology and chemical composition of the as-prepared samples. A high-resolution transmission electron microscope (HR-TEM) (JEOL JEM 2100) was used to infer the structural characterization of the synthesized materials. X-ray photoelectron spectroscopy (XPS, ESCALAB 250XI, Germany) was used to understand the valence states of the elements in the prepared $NiCoTe_2$/MXene composite. The electrochemical workstation (Autolab PGSTAT302N, Netherlands) was used to study the electrochemical properties and energy storage performance of the developed composites.

Specific capacity calculation

The specific capacity (Q, in the unit of mAh g^{-1}) was calculated from the integral area of the CVs curves based on the following eqn. (S1).[1]

$$Q = \frac{Idv}{2 \times 3.6 \times m \times V} \quad \text{..... (S1)}$$

The specific capacity (Q, in the unit of mAh g^{-1}) was also calculated from the GCD discharge curves based on the following eqn. (S2). [2]

$$Q = \frac{I \times \Delta t}{m} \text{ /3.6 ..... (S2)}$$

Where 'I' is the current, Δt is the discharge time, U is the testing voltage range, and m is the mass of the active material.

Specific energy and specific power calculation

The specific energy (E) (Wh kg^{-1}) and specific power (P) (W kg^{-1}) of the composites were calculated based on the following eqns. (S3 & S4).

$$E = \left(\frac{1}{m}\int_0^{t_d} iV\, d_t\right) \quad \text{..... (S3)}^3$$

$$P = 3600 \times \frac{E}{t_d} \quad \text{..... (S4)}^3$$

Where m is the total mass of the device, i is the discharge current, V is the potential, and t_d is the discharge time.

Charge balance calculation

Charge balance of electrodes in asymmetric supercapacitors

The charge must be balanced in an asymmetric supercapacitor device using the relationship $Q_+ = Q_-$ where Q_+ is the charge stored at the positive and Q_- is the charge stored at the

negative electrodes. The charge storage by each electrode depends on the specific capacity (Q), the potential range for the charge/discharge process (ΔE), and the mass loading of the active material (m). [4]

Coulombic efficiency calculation

The coulombic efficiency was calculated by using the following eqn. (S5). [5]

$$\eta(\%) = \frac{t_d}{t_c} \times 100 \quad \text{…….. (S5)}$$

Where η (%) is Coulombic efficiency, t_d (s) represents discharging time, and t_c (s) represented

charging time.

Capacity retention calculation

The capacity retention was calculated by using the following eqn. (S6). [5]

$$C_R(\%) = \frac{C_F}{C_I} \times 100 \quad \text{……. (S6)}$$

Where C_R (%) is capacity retention, C_F represents the final capacity, and C_I is the initial capacity.

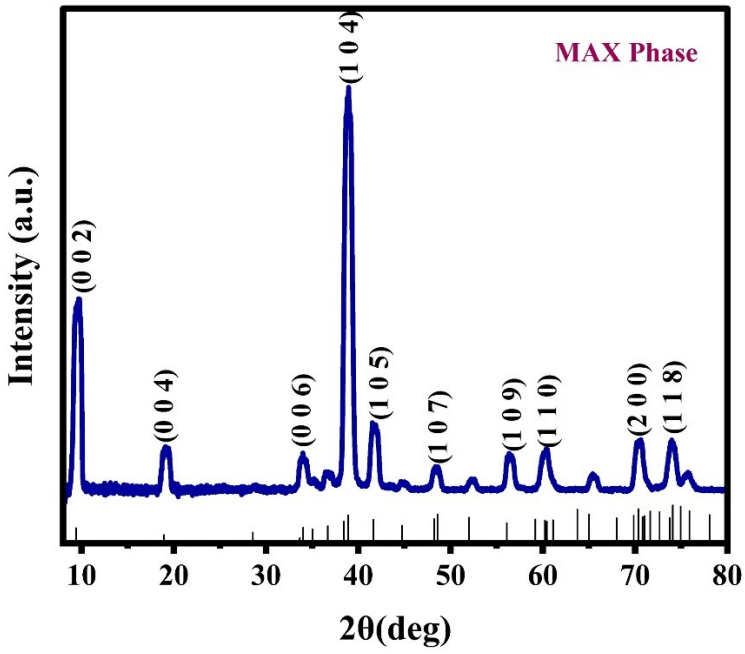

Fig. S1 XRD pattern of Ti_3AlC_2 MAX phase.

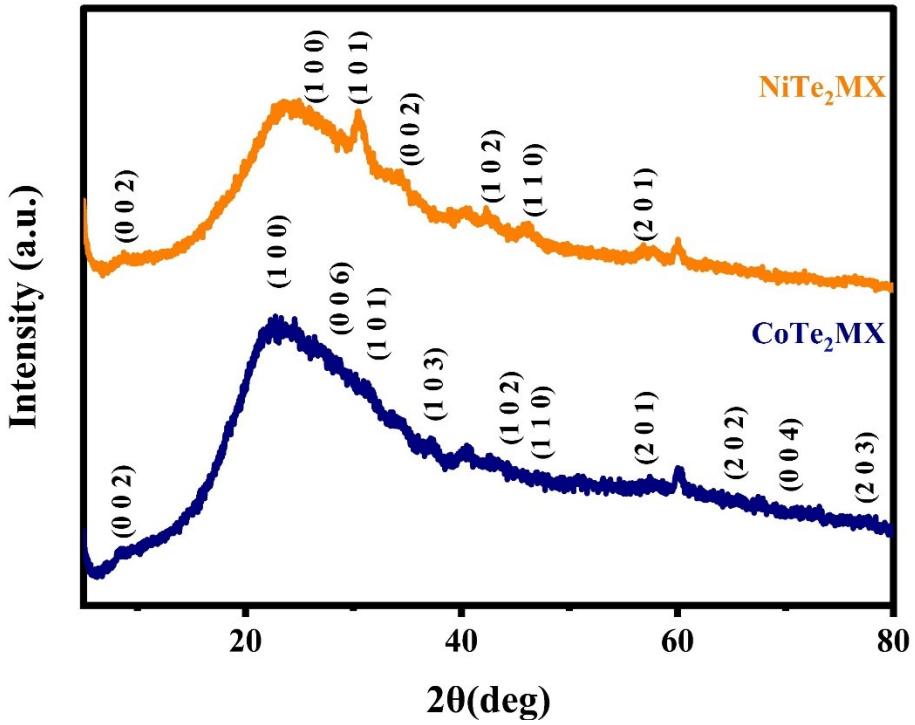

Fig. S2 XRD patterns of $NiTe_2MX$ and $CoTe_2MX$ composites.

Table S1: The 2θ and hkl values of $NiCoTe_2$ and MXene derived from XRD patterns.

$NiCoTe_2$	
2Ɵ	hkl values
26.436°	(1 0 0)
31.295°	(1 0 1)
33.373°	(0 0 2)
42.904°	(1 0 2)
53.86°	(2 0 0)
58.282°	(1 0 3)
70.084°	(0 0 4)
74.376°	(2 1 0)
12.74°	(0 2 1)
19.75°	(0 0 1)
21.11°	(1 1 1)
27.90°	(1 0 0)
MXene	
9.436°	(0 0 2)
18.937°	(0 0 4)
28.572°	(0 0 6)

18.93°	(0 1 9)
36.689°	(1 0 3)
38.418°	(0 0 8)
54.29°	(1 0 8)
56.06°	(1 0 9)
67.962°	(1 1 6)

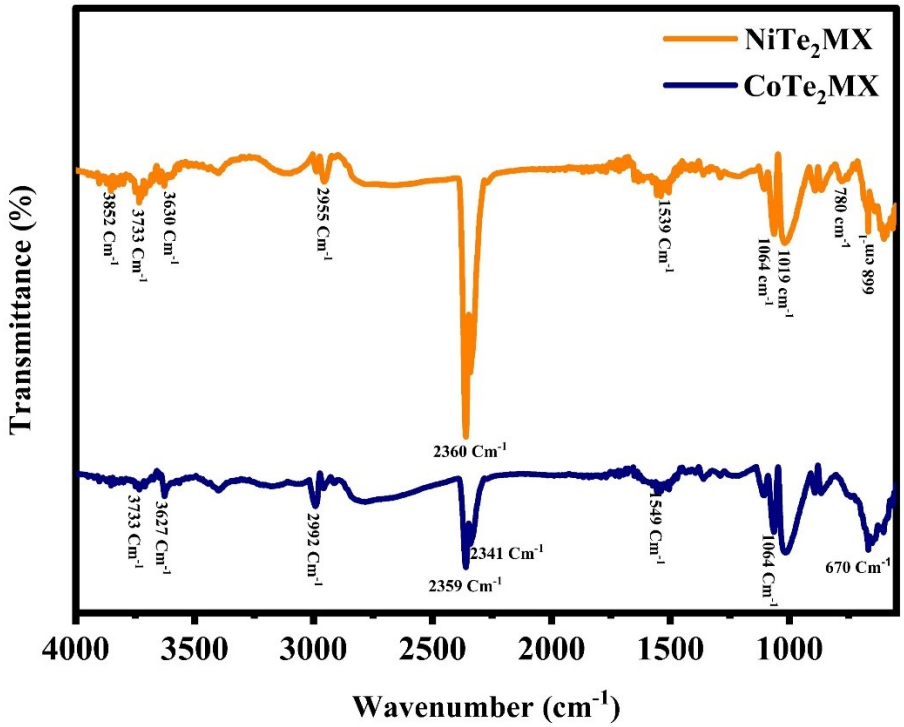

Fig. S3 FTIR spectra of $NiTe_2MX$ and $CoTe_2MX$ composites.

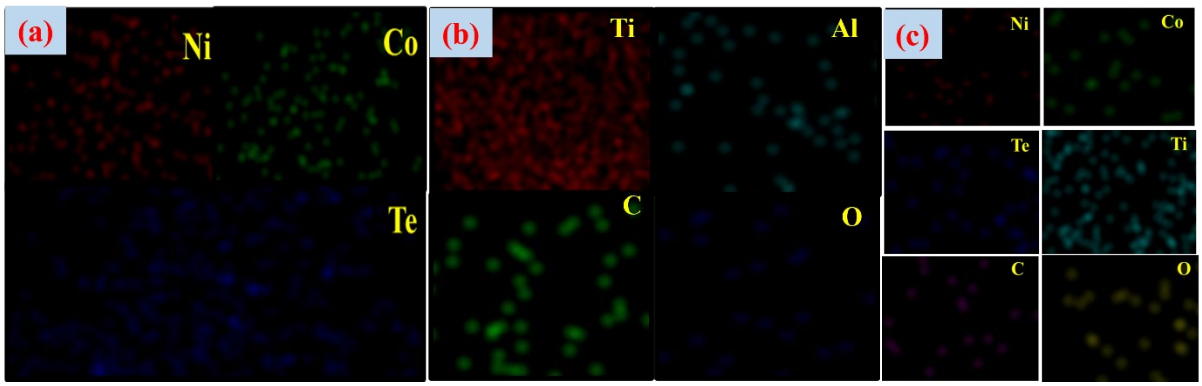

Fig. S4 Elemental mapping of (a) $NiCoTe_2$, (b) MXene, and (c) $NiCoTe_2$/MXene composites.

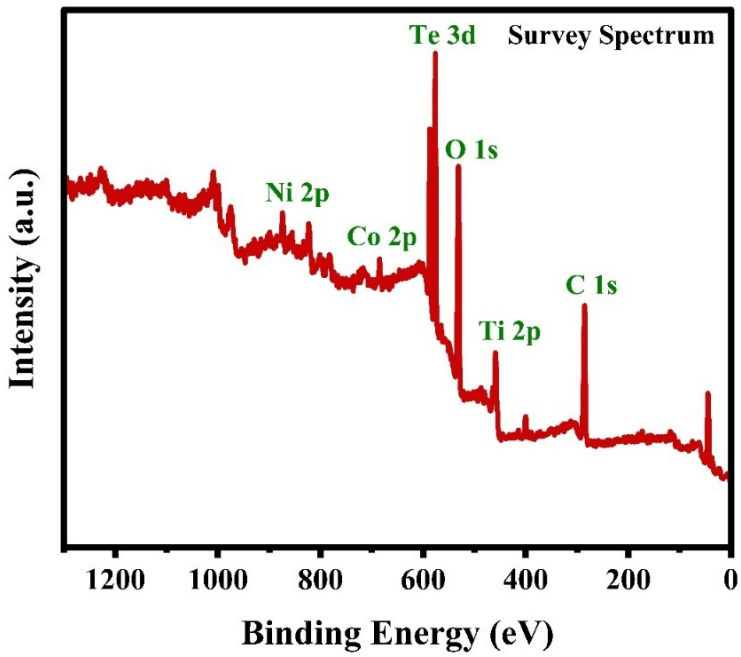

Fig. S5 XPS survey spectrum of $NiCoTe_2$/MXene composites.

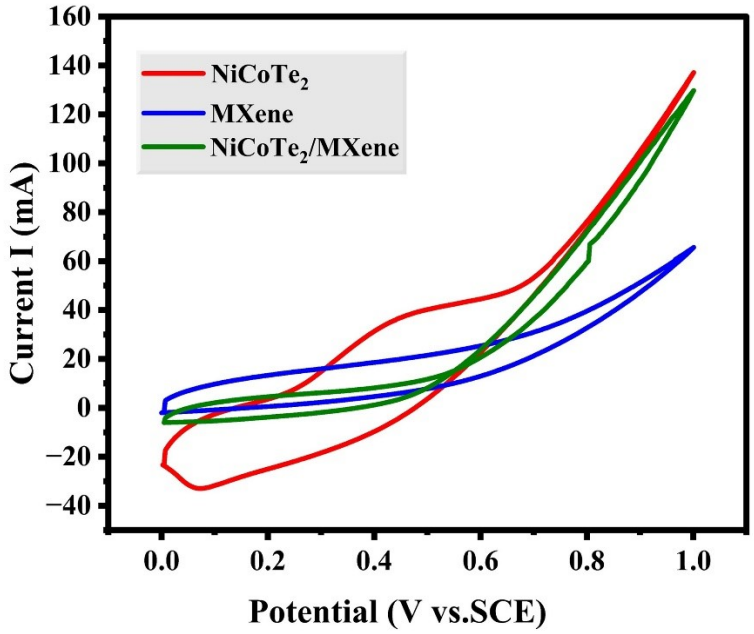

Fig. S6 CVs recorded in the positive window for $NiCoTe_2$, MXene, and $NiCoTe_2$/MXene composite in 6.0 M KOH.

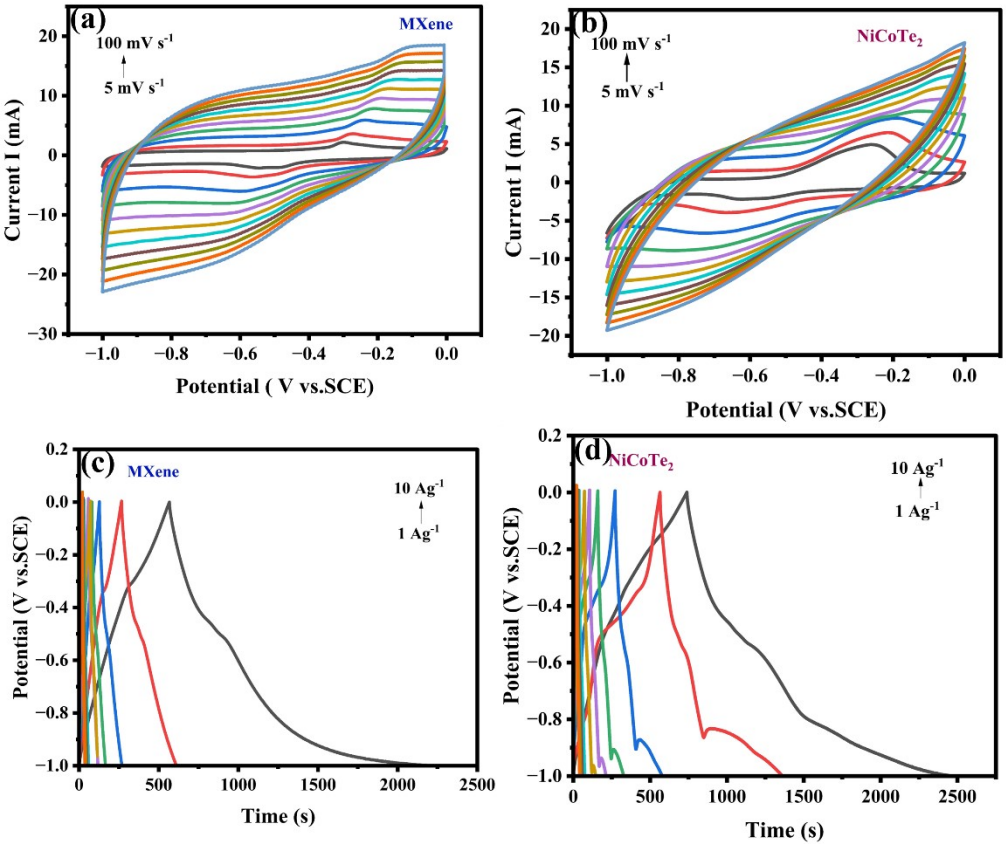

Fig. S7 CVs recorded for (a, b) MXene, $NiCoTe_2$ coated on GS electrodes with increasing scan rates from 5 to 100 mV s^{-1} in 6.0 M KOH, GCD performances of MXene and NiCoTe (c, d) performed at different current densities (1-10 Ag^{-1}).

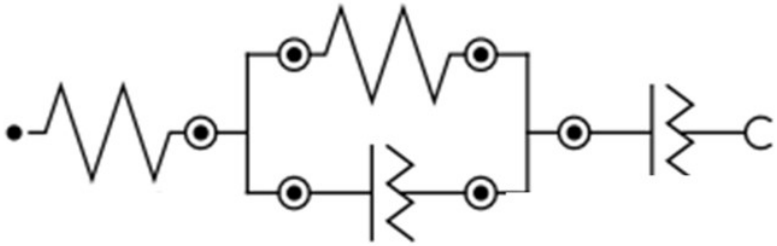

Fig. S8 Equivalent circuit fitted for $NiCoTe_2$/MXene composite.

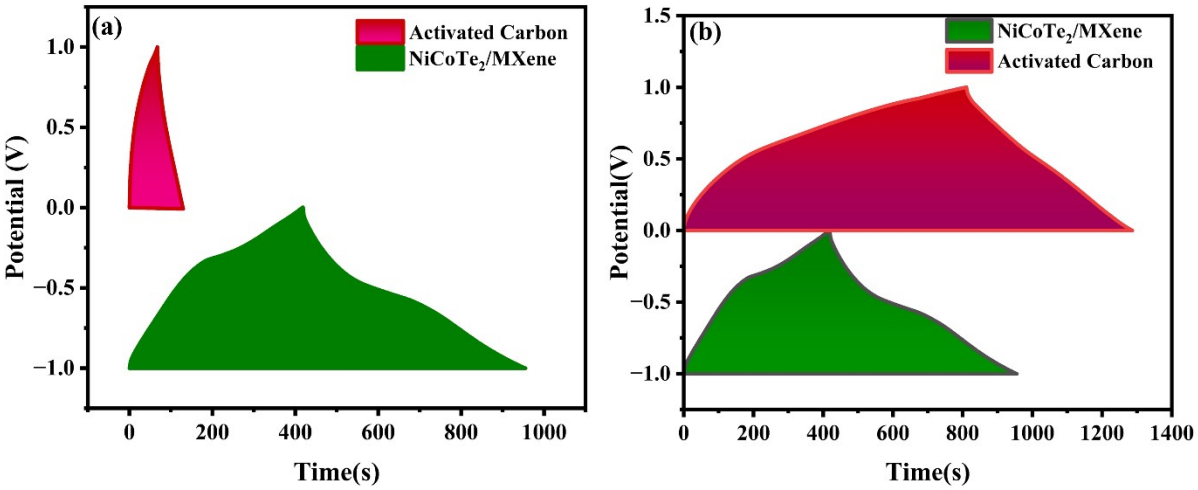

Fig. S9 Two electrode studies of $NiCoTe_2$/MXene||AC asymmetric supercapacitor (a-b) mass balance of GCD curves.

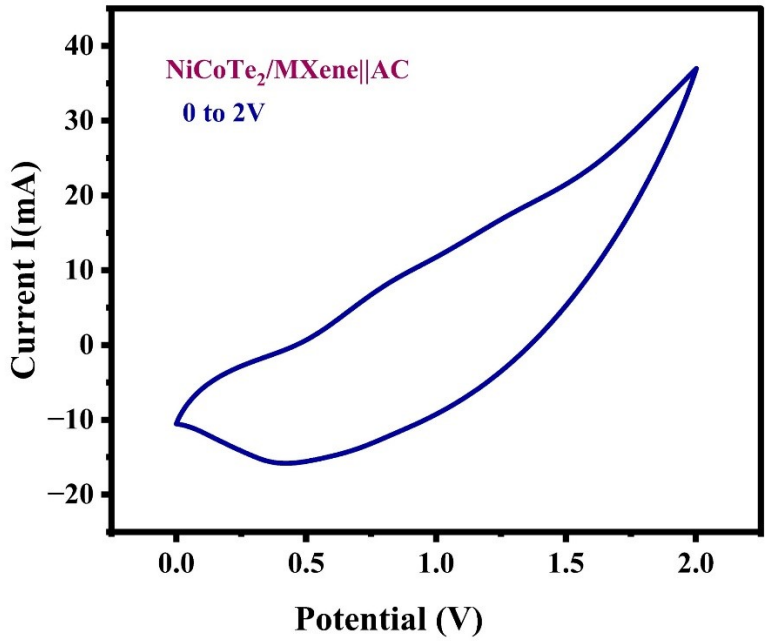

Fig. S10 CV curve of $NiCoTe_2$/MXene||AC electrode for the extented potential window from 0 to 2.0 V.

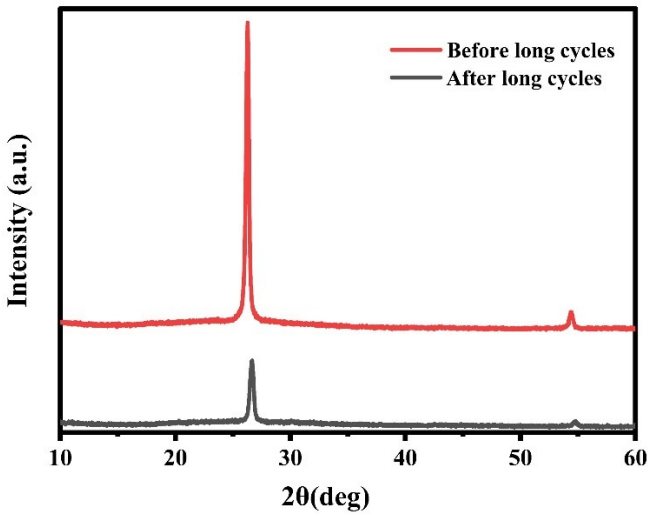

Fig. S11 Pre and post-cycled XRD patterns of $NiCoTe_2$/MXene composites.

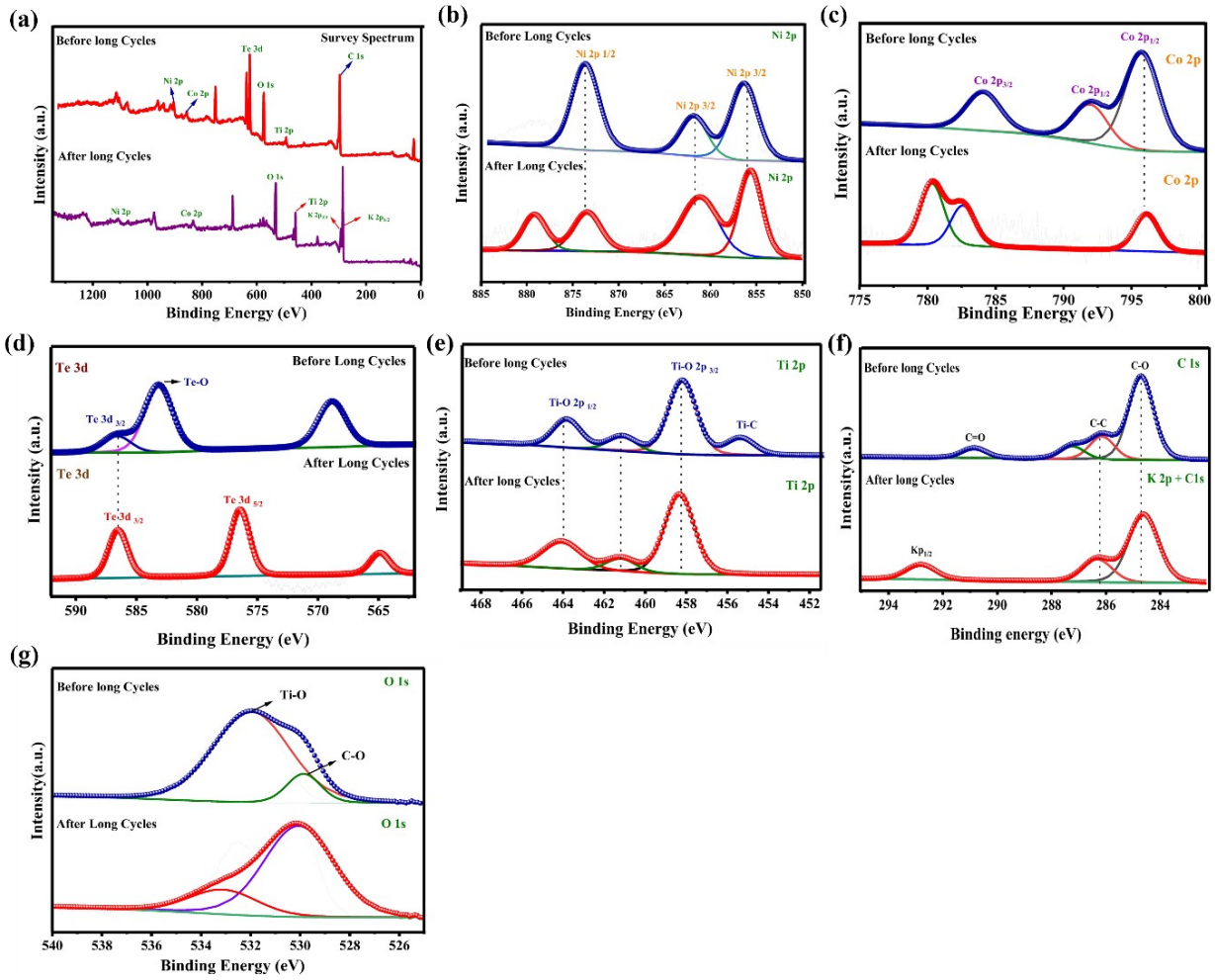

Fig. S12 Pre and post cycled XPS survey spectra of $NiCoTe_2$/MXene composite (a), post cycled XPS of individual element of (b) Ni 2p (c) Co 2p (d) Te 3d (e) Ti 2p (f) C1s (g) O 1s.

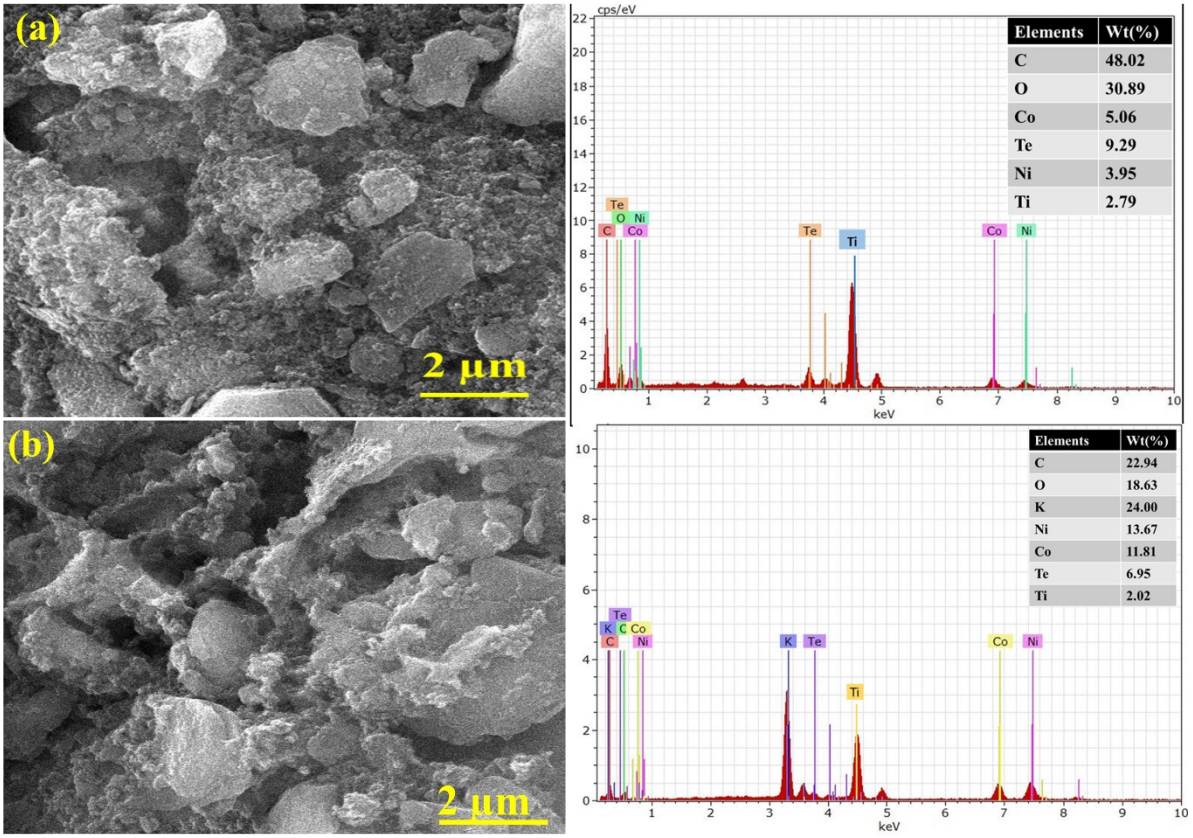

Fig. S13 SEM and EDAX images of (a) before and (b) after long cycles of $NiCoTe_2$/MXene composite.

Table S2. Comparison of $NiCoTe_2$/MXene||AC modified graphite sheet electrode concerning specific capacity, power, and energy densities to those reported elsewhere.

Electrode	**Electrolyte**	**Specific capacitance**		**Power density**	**Energy density**	**Comments** (Solid-state electrolyte)	**Ref**
		Three electrode 1 A g^{-1} (mAh g^{-1})	**Two electrode 1 A g^{-1}** (mAh g^{-1})				
NiSb/NiTe[a]	6.0 M	519.4	430.5	750 µW cm^{-2}	224.6 µWh cm^{-2}	Not used	6
CoTe@rGO[b]	3.0 M KOH	225.16	31.27	799.91 W kg^{-1}	40.04 Wh kg^{-1}	Not used	7
MCTe/NFTe@ NiF[c]	3.0 M KOH	223.36	144.98	799.98 W kg^{-1}	51.55 Wh kg^{-1}	Not used	8
$NbTe_2$@rGO[d]	2.0 M KOH	409.7	138.3	285 W kg^{-1}	22 Wh kg^{-1}	Not used	9
$NiTe_2$-Co_2Te_2@rGO[e]	1.0 M KOH	223.6	64	800 W kg^{-1}	51 Wh kg^{-1}	Not used	10
CoTe/Co/CoO[f]	2.0 M KOH	139.17 at 5 mA cm^{-2}	-	616.26 W kg^{-1}	35.29 Wh kg^{-1}	Not used	11
NiTe:Co[g]	3.0 M KOH	457.1	242.4		36.8 Wh kg^{-1}	Not used	12
NiLaTe[h]	2.0 M KOH	95.7	60.0	5,488.7 W kg^{-1}	45.5 Wh kg^{-1}	Used	13
$NiCoTe_2$ NRs[i]	3.5 M KOH	120 at 0.5 A g^{-1}	106 at 0.5 Ag^{-1}	905 W kg^{-1}	43 Wh kg^{-1}	Not used	14
Te NTs@CoMgTe MTs)[j]	2.0 M KOH	42.4	56.3	6,857.1 W kg^{-1}	42.2 Wh kg^{-1}	Used	15
Co-Fe decorated	4.0 M KOH	1,119.2	179.2	1,138.2	62.1	Not used	16

Te[k]				W kg^{-1}	Wh kg^{-1}		
Co-decorated Te nanotubes	4.0 M KOH	77	40.83	2,294 W kg^{-1}	51.1 Wh kg^{-1}	Not used	[17]
CF@$CoTe_2$-$NiTe_2$[m]	6.0 MKOH	261.4	131.1	750 W kg^{-1}	41 Wh kg^{-1}	Not used	[18]
$CoTe_2$/ZnTe/$Ti_3C_2T_x$[n]	4.0 M KFSI in dimethoxyethane	137.0 at 10 Ag^{-1}	175.3 at 10 Ag^{-1}	837.2 W kg^{-1}	220.2 Wh kg^{-1}	Not used	[19]
V_2CT_x@$CoMn_2O_4$[o]	1.0 M H_2SO_4	158.3	47.2	440 W kg^{-1}	62 Wh kg^{-1}	Not used	[20]
Mo_2CT_x/Ni, Co-MOF[p]	1.0 M KOH	16.1	-	293 W kg^{-1}	22 Wh kg^{-1}	Used	[21]
$NiCoTe_2$/MXene||AC	**6.0 M KOH**	**582**	**298**	**11,520 W kg^{-1}**	**233 Wh kg^{-1}**	**Used & discussed**	**This Work**

[a]NiSb/NiTe/Ni -nickel antimony/nickel telluride on nickel foam. [b]CoTe@reduced graphene oxide. [c]MnCoTe/NiFeTe on a NiF. [d]Fabrication of rGO with niobium telluride ($NbTe_2$). [e]Spherical $NiTe_2$-Co_2Te_2 grown on the rGO. [f]$Co(OH)_2$ nanosheet transformed into CoTe, metallic Co, and CoO composite. [g]NiTe: Co nanoparticles supported on nickel foam. [h]The NiTe MFs and La_2Te_3 microrods (MRs). [i]nickel cobalt telluride nanorods. [j]tellurium nanotubes, cobalt magnesium telluride microtubes. [k]Cobalt-iron (CoFe) decorated tellurium nanotubes. [l]Co-decorated Te nanotubes. [m]nickel-cobalt telluride. [n]Cobalt telluride/zinc telluride ($CoTe_2$/ZnTe) onto MXene nanosheets. [o]V_2C@$CoMn_2O_4$ Vanadium carbide MXene on cobalt manganese oxide. [p]Ni, Co bimetallic metal−organic frameworks (Ni, Co-MOF) on Mo_2CT_xMXene.

References

1 R. Palanisamy, D. Karuppiah, S. Venkatesan, S. Mani, M. Kuppusamy, S. Marimuthu, A. Karuppanan, R. Govindaraju, S. Marimuthu, S. Rengapillai, M. Abdollahifar, A.K. Anbalagan, R. Perumalsamy, *Colloids Interface Sci. Commun.,*2022, **46,** 100573.

2 Z. Zhu, Z. Liu, Y. Yin, Y. Yuan, Y. Meng, T. Jiang, Q. Peng, W. Wang, W. Chen, *Nat. Commun.,* 2022, **13,** 2805.

3 Mathis, T. S.; Kurra, N.; Wang, X.; Pinto, D.; Simon, P.; Gogotsi, Y., *Adv. Energy Mater.* 2019**,** ***9***, 1902007.

4 K.A. Owusu, L. Qu, J. Li, Z. Wang, K. Zhao, C. Yang, K.M. Hercule, C. Lin, C. Shi, Q. Wei, L. Zhou, L. Mai, *Nat. Commun.,* 2017, **8**, 14264.

5 M. Fallah barzoki, S. Fatemi, M.R. Ganjali, *J. Energy Storage.*, 2022, **55,** 105545.

6 H. Zhao, X. Hu, H. Kang, F. Feng, Y. Guo, Z. Lu, *ACS Omega*, 2024, **9,** 2597–2605.

7 T. Wang, Y. Su, M. Xiao, M. Zhao, T. Zhao, J. Shen, *Trans. Tianjin Univ.*, 2022, **28,** 112–122.

8 T.S. Panah, M. Shirvani, S.S.H. Davarani, *J. Colloid Interface Sci.,* 2025, **678,** 1012–1024.

9 M. Hussain, A.M.M. Abdelbacki, M. Saleem, M. Aslam, M. Ali, *J. Phys. Chem. Solids,* 2024, **196,** 112354.

10 M. Farshadnia, A.A. Ensafi, K.Z. Mousaabadi, B. Rezaei, M. Demir, *Sci. Rep.*, 2023, **13,** 1364.

11 M. Chen, Y. Lu, W. Li, P. Qi, G. Liu, S. Wang, Z. Chen, Y. Tang, *Electrochim. Acta,* 2022, **413,** 140101.

12 B. Ye, M. Huang, L. Fan, J. Lin, J. Wu, *J. Alloys Compd.,* 2019, **776,** 993–1001.

13 P. Bhol, P.B. Jagdale, N. Barman, R. Thapa, M. Saxena, A.K. Samal, *J. Energy Storage,* 2023, **65,** 107286.

14 M. Manikandan, K. Subramani, S. Dhanuskodi, M. Sathish, *Energy Fuels*, 2021, **35**1, 2527–12537.

15 P. Bhol, P.B. Jagdale, A.H. Jadhav, M. Saxena, A.K. Samal, *ChemSusChem,* 2024, **17,** 202301009.

16 P. Bhol, S. Swain, A. Altaee, M. Saxena, A.K. Samal, *Mater. Today Chem.,* 2022, **24,** 100871.

17 P. Bhol, S. Swain, S. Jena, K. Bhatte, C.S. Rout, M. Saxena, A.H. Jadhav, A.K. Samal, *ACS Appl. Nano Mater.,* 2021, **4,** 9008–9021.

18 C. Shi, Q. Yang, S. Chen, Y. Xue, Y. Hao, Y. Yan, *ACS Appl. Nano Mater.,* 2022, **5,** 2817–2825.

19 L. Pan, R. Hu, Y. Zhang, D. Sha, X. Cao, Z. Li, Y. Zhao, J. Ding, Y. Wang, Z.M. Sun, *Nanomicro Lett.,*2023, **15,** 225.

20 J. Vigneshwaran, A. Sakthivel, A. Kumari, R.L. Narayan, V. Chakkravarthy, D. Ghosh, S.P. Jose, *ACS Appl. Mater. Interfaces,* 2024, **16**, 67553-66.

21 J. Liu, Q. Xia, L. Wang, Q. Hu, N.M. Shinde, A. Zhou, *ACS Appl. Mater. Interfaces*, 2024, **16,** 49380-91.